Rocket Exhaust Impact on Stratospheric Ozone

Prepared for:

U.S. Air Force Space and Missile Systems Center
Environmental Management Branch
SMC/AXFV

under
Contract F09603-95-D-0176-0007

Prepared by:

Peter D. Lohn, Eric P. Wong, Tyrrel W. Smith, Jr.
TRW Space & Electronics Group

John R. Edwards and Daniel Pilson
Environmental Management Branch

Submitted by:

TRW Space & Electronics Group

30 September 1999

Rocket Exhaust Impact on Stratospheric Ozone

Prepared for:

U.S. Air Force Space and Missile Systems Center
Environmental Management Branch
SMC/AXFV

under
Contract F09603-95-D-0176-0007

Prepared by:

Peter D. Lohn, Eric P. Wong, Tyrrel W. Smith, Jr.
TRW Space & Electronics Group

John R. Edwards and Daniel Pilson
Environmental Management Branch

Submitted by:

TRW Space & Electronics Group

Approved by:

John J. Lamb, Ph.D.
Program Manager

30 September 1999

ROCKET EXHAUST IMPACT ON STRATOSPHERIC OZONE

CONTENTS

1. Introduction and Summary

The Environmental Management of the Space & Missile Systems Center (SMC) has set out to evaluate the depletion of stratospheric ozone caused by Air Force space activities. Earlier work supported by SMC included an assessment of the impact of deorbiting debris on stratospheric ozone (Reference 1.1) and the potential for reduction of ozone destruction by use of alternate propellants for launch vehicle rocket engines (Reference 1.2). A more recent effort, supported by SMC, addressed the impact of rocket exhaust on stratospheric ozone (Ref. 1.3). This work was an extension of an earlier study reported in Reference 1.4. The methodology described in Ref. 1.3 and 1.4 allows a quantitative assessment of the destruction of stratospheric ozone by rocket exhaust. The present study describes development and application of upgrades to the methodology by including and multiple engine effects as well as the effects of stratospheric winds.

The primary results of the present study are summarized as follows:

1) Enhancement of HCl dissociation in the plume by Mach disc, barrel shock and multiple engine interaction effects is relatively small: about 10% more than by afterburning alone. The previous assessment of NO_x (used in reference 1.3 & 1.4) has implicitly included Mach disc effects. The present work shows an increase of less than 1% increase in NO_x levels caused by multiple engine interaction effects.

2) Multiple engine interaction effects on stratospheric ozone have been quantified by analysis. The results have been folded into an upgraded model. The effects are relatively small and account for less than a 10% increase in local ozone depletion. This result demonstrates by analysis that single plume assessment (the entire exhaust is considered to be a single plume from a thruster with the total launch thrust and total exhaust flow rate) of stratospheric ozone depletion by rocket exhaust impact is sufficiently accurate for a multiple engine launcher.

3) The effects of wind shear on the diffusion/mixing of the exhaust plume are addressed by analysis (full Navier-Stokes models). This effort leads to a modification of the cold wake diffusion model that is within the range of that suggested by the data and outlined in References 1.3 and 1.4.

4) Local ozone depletion caused by a solid rocket launch vehicle is calculated for several altitudes in the stratosphere. The calculations take into account afterburning, barrel shocks, Mach disks, impingement shock effects resulting from multiple engines and the effects of wind shear. The results compare well with recent fly-through measurements taken in the exhaust plume of a Titan IV launch.

2. Multiple Engine Exhaust Plume Effects

Introduction

Recent concerns over the potential depletion of stratospheric ozone by rocket exhausts have prompted a number of analytical investigations and field measurements regarding the destruction mechanism (References 1.3, 1.4 & 2.1) and the existence of a local ozone hole is predicted by these analytical investigations. In our study (Ref. 1.3) of a Titan class single solid rocket plume which include the detailed analysis of the rocket plume chemistry and gas dynamics, and the cold plume dispersion that follows, it was found that a local hole of significant ozone depletion can form as a result of chemical interactions with the exhaust. Furthermore, we have discovered that the afterburning region in the plume plays a predominant role in converting exhaust product HCl into Cl (or Cl_2). As a result of Cl/Cl_2 production by afterburning, ozone in the stratosphere is destroyed through the chlorine catalytic mechanism.

Much of the basic hot and cold plume chemical kinetics work have already been reported by the authors (Ref. 1.3, 1.4). This report, however, will concentrate on the study of the effects on stratospheric ozone caused by launch vehicles with multiple solid rocket motors, such as the U.S. Space Shuttle main engine and Titan III &IV rocket motors.

To understand the difference between a single and multiple engine let us first examine the common as well as distinct flow features found in these two cases types of plumes as illustrated schematically in Figures 2.1 and 2.2. Figure 2.1 shows several distinct features found only in supersonic jets, namely, the alternating or periodic nature of the flow in the imbedded shock structures. These features can be easily understood from a compressible gas dynamics perspective. In most rocket exhaust, the gas pressure at the exit plane of the nozzle is higher than the ambient, thus creating an under-expanded supersonic jet. Upon exiting the nozzle, the exhaust plume expands in order to match the lower pressure in the surrounding thereby creating the expansion waves (i.e., pressure pulse) at the exit. The expansion waves propagate downstream and some location will be finally reached where the waves intercept the constant pressure ambient boundary. Upon reflection from the plume boundary, the incident expansion waves become compressive in order to match a higher local pressure. Due to the curvature of the plume boundary these reflected compressive waves tend to coalesce downstream forming the barrel shock shown in the figures. If the barrel (or oblique) shock is strong meaning that the shock angle relative to the streamline is almost normal, a normal shock will be formed on the centerline axis of the plume. Commonly known as the Mach disc this normal shock has a disk shape in an axisymmetric plume. The Mach disc is important in the current analysis because it is a strong normal shock and the flow downstream of is subsonic with high temperature and pressure. The presence of subsonic region provides an environment in which ambient nitrogen can be transformed into NO_x through the Zeldovich mechanism. Depending on the pressure ratio between that of the exhaust exit and ambient, the pattern of barrel-shock and Mach disc combination may repeat several times thus forming a diamond crystal shape pattern called shock diamond (which ultimately weakens with mixing).

Figures 2.2a & 2.2b sketches the top and side view of the flow structure of a multiple rocket launcher. Similar to the single nozzle plume, the repeating element of the barrel-shock and Mach disc, i.e. the shock diamond, can be observed in multiple nozzle plumes. From the top view the shock diamond is displaced off the plume axis due to the presence of the neighboring jet. From the side view however, the multiple nozzle plume is seen to have an additional shock wave located in the symmetry plane of the two neighboring supersonic plumes namely the impingement shock caused by turning the plume towards the axial direction (Fig. 2.2b).

Having described the flow features of a single and multiple nozzle plume we return to the discussion of the multiple plume effects on stratospheric ozone. The effects not accounted for in a single nozzle plume may be understood in two different ways: (1) In the multiple plume case, due to less three-dimensional relief effect as compared to the single plume case, the shock strength of the Mach disc and the barrel shocks are expected to be stronger, therefore allowing higher rates of chlorine and NO_x production. The presence of stronger shocks on ozone depletion must be accounted for in the multiple plume case (2). The additional shock present in the multiple plume case creates another region in which favorable conditions, i.e., high temperature, high pressure, exist where significant HCl conversion and NO_x production can take place.

To evaluate the extent that these complicated shock structures, (barrel shock, Mach disc and impingement shock) can contribute in the production of ozone depletion one needs to assess the kinetic effects immediately downstream of these shock regions where the temperature and pressure are high. In the presence of high concentration of unburned H_2 and H_2O free radicals (e.g., H & OH) may be formed according to the following thermal dissociation mechanism:

$$H_2 + M \rightarrow 2H + M \qquad (2\text{-}1)$$

$$H_2O + M \rightarrow H + OH + M \qquad (2\text{-}2)$$

$$HCl + M \rightarrow H + Cl + M \qquad (2\text{-}3)$$

Reaction (3) provides a direct route for the production of atomic chlorine which again may be important in the high temperature regions (as high activation energy, $E_A \sim 82$ kcal/mole, would show). On the other hand, Reactions (1) and (2) are thermal decomposition reactions of that generate H & OH with activation energies of approximately 100 kcal/mole. At these high activation energy levels these reactions are favored in the high temperature regions downstream of these exhaust shocks. As free radicals, H and OH are generated, the HCl present in the exhaust will dissociate according to the mechanism we have discovered in our previous studies (Ref. 1.3 & 1.4). Or more specifically,

$$HCl + H \rightarrow H_2 + Cl \qquad (2\text{-}4)$$

$$HCl + OH \rightarrow H_2O + Cl \quad (2\text{-}5)$$

(This significance of this mechanism has since been confirmed experimentally by Burke & Zittel: Ref. 2.2).

In addition to the chlorine production mechanism we may have NO_x formation with nitrogen directly transported from the exhaust, or indirectly entrained from the ambient. Combining with the entrained oxygen, NO_x is produced according to the Zeldovich mechanism:

$$O_2 + M \rightarrow 2O + M \quad (2\text{-}6)$$

$$O + N_2 \rightarrow NO + N \quad (2\text{-}7)$$

$$N + O_2 \rightarrow NO + O \quad (2\text{-}8)$$

Approach

To assess the importance of these chemistry effects the production of chlorine from HCl and nitrogen oxide from thermal process must be quantified. For that purpose a detailed (but computationally extensive) analysis may be used which would include the simultaneous consideration of shock capturing in gas dynamics and finite rate of reaction in chemistry. Such a detailed approach is not adopted here however. A two step approach, which essentially decouples the gas dynamics from chemical kinetics, can be used to provide a sufficiently accurate result. Specifically, computational fluid dynamics models (SPF and the Fluent/RAMPANT) computer codes were used to determine the complicated flowfield/shock structures. The production of chlorine and NO_x is characterized by performing one-dimensional streamtube detailed finite rate kinetics involving the exhaust and ambient gases of the exhaust plume. The chemistry effects are evaluated in terms of chlorine and NO_x production. Accurate prediction of these species can be made with a detailed modeling of the kinetics involving exhaust and ambient species. The calculation can proceed along representative streamlines in the shock region. Alternatively, conservative estimates of the production rates can also be made by evaluating the half-lives of the radical generating reactions involving exhaust species H_2, H_2O and HCl, and the flow transit times. Thus if the flow transit time is long compared to reaction time, complete conversion of HCl in the flow is expected.

As a study example, the SRM of the Titan IIIC exhausting in the stratosphere at 20 Km was selected. The following summarizes the nozzle exit plane conditions (Reference 2.3) and ambient conditions used in our calculations (See Tables 2-1 through 2-3).

Table 2-1. Exit Plane Conditions

Radius (m)	1.35
Temperature (^{o}K)	1921
Static Pressure (atm)	0.702
Speed (m/sec)	2590

Table 2-2. Species Concentration (in mole fraction)

Species	Concentration (mole fraction)
Al_2O_3	0.0717
CO	0.2452
CO_2	0.0181
Cl	0.0012
H_2	0.3136
H	0.0032
H_2O	0.1051
HCl	0.1500
N_2	0.0805
NO	0.0067

Table 2-3. Ambient Conditions

Temperature (^{o}K)	216
Static Pressure (atm)	0.0545
Cruise Speed (m/sec)	690

Results

Figures 2.3-2.5 show the near-field pressure, Mach number and temperature profile for a single non-intersecting plume using the SPF computer model (the plume is exhausting from left to right). For illustration purpose the radial dimension of the plume is greatly expanded so that flow structures can be easily identified. In the pressure contour plot, Figure 2.3, the out-most contour is fixed at a pressure of 0.05 atmosphere, which is the same as the ambient pressure at 20 km. Therefore one may consider the out-most contour being that of the actual ambient plume boundary. Examination of these figures shows two principal features. First we note the spatially periodic nature of the flow with expansion and contraction of the flow area corresponding to the increase and decrease of plume size. As discussed in the previous paragraphs, the increase and decrease in area is a ramification of the alternating expansion and compression waves brought on by the wave reflection on the constant pressure boundary. The second principal feature is the repeating pattern interacting shocks. Two distinct shock diamonds (which include barrel shock and Mach disc combination) can be seen on Figure 2.4. Figure 2.4 shows the local Mach number profile and it clearly shows the presence of the Mach disk. The first Mach disc is located at the axial location of approximately 20 nozzle exit radii (R_e) as indicated by the appearance of the subsonic region in the supersonic jet. Figure 2.5 shows the temperature profile of the flow and it shows at least three distinct high temperature regions. The first region coincide with the subsonic region just downstream of the Mach disc at ~30 R_e. The second region stands off at ~1-2 R_e from the centerline just above the Mach Disc. This second region coincides with the downstream region of the first barrel shock. The third high temperature region is seen to occur at ~50 R_e, behind the second Mach disc.

The temperature behind these shocks reaches ~3800 K. At these high temperatures extensive thermal dissociation (in accordance with reactions 1-3) will occur. In fact, using the calculated local flow conditions downstream of these shock structures the reaction half-life for H_2, H_2O and HCl are found to be on the order of 1 millisecond as shown in Table 2-4. Whereas the flow transit time behind the barrel shock and Mach disk are found to be 13.2 and 18.6 msec, respectively. Therefore the HCl flowing through these high temperature regions completely (or very nearly completely) dissociated.

Table 2-4. Thermal Dissociation Half Life behind the Mach Disc (in millisecond)

Reaction	1	2	3
Half life, ms	0.34	0.02	1.03

Figure 2.6 shows the near-field temperature profile in the symmetry plane of the twin nozzle Titan exhaust plumes as calculated by the Fluent/RAMPANT computer code. Due to the coarseness of the computational grid detailed shock structures illustrated in Figure 2.2 & 2.2b are not clearly resolved in these calculations. The three-dimensional Navier-Stokes calculation was set up to quantify the multiple plume interaction effects where the temperature is calculated to

reach 2300K in the interaction region. As shown in Table 2-5, the half lives for reactions 1-3 at this temperature are approximately 5 orders of magnitude longer than those in the barrel shock and Mach disk regions where the temperature is higher (Table 2-5). The interaction region reaction times are long compared to the flow transit time in this region (~ 1.9 msec) suggesting that thermal dissociation reactions are probably unimportant in the reaction region. However with the entrainment of the ambient oxygen, significant afterburning may take place in the impingement region where free radicals are formed through the H_2/O_2 mechanism. In the presence of the free radicals H and OH, production of chlorine can proceed according to reactions 4-5 (Ref. 1.4). At 2300 K however, the production of nitric oxide is not expected to be significant in this region.

Table 2-5. Thermal Dissociation Half Life in the Impingement Region (milliseconds)

Reaction	1	2	3
Half-life	960	281	841

Conclusion

We have identified three high temperature regions in a twin nozzle rocket plume where additional production of chlorine and NO_X (other than the afterburning region) can be significant. These three flow features, the barrel shock, Mach disc and the impingement shock, are regions commonly found in solid rocket exhaust plumes. For a Titan III twin nozzle plume however, the current analysis shows a 4.5 % , 5.0% and 0.6% (by mass) of the total mass flow flowing through the Mach disc, barrel shock and impingement shock respectively. In view of the short reaction times required for complete reaction, most of the HCl in these regions is expected to be fully converted. Therefore a maximum enhancement of about 10% (in addition to afterburning) is expected for a Titan IIIC class of twin nozzle plumes. The production of NO_x however is mostly limited to the interaction region and the contribution to the overall ozone depletion is small, i.e., ~ 0.08%.

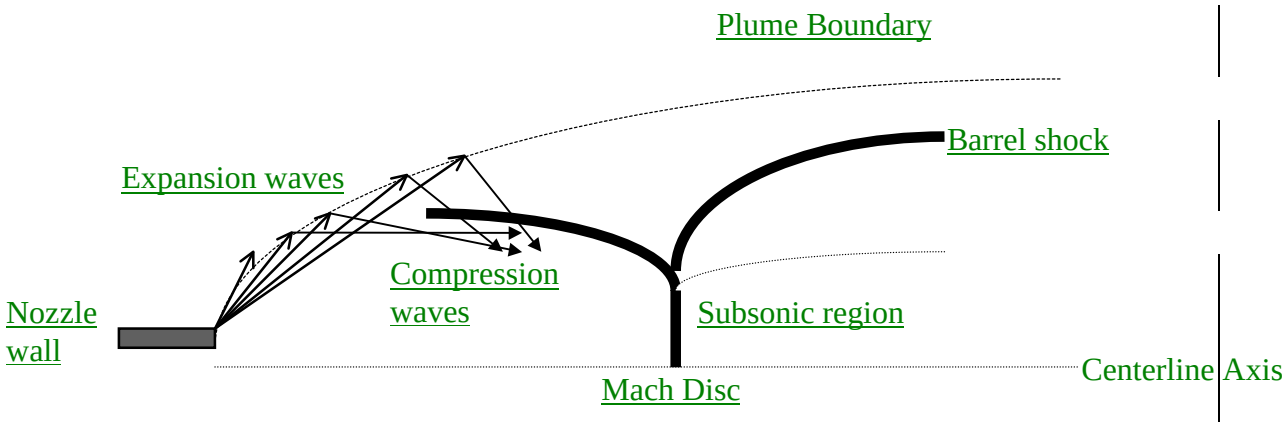

Figure 2.1 – Flow Structure of a Supersonic Single Nozzle Plume

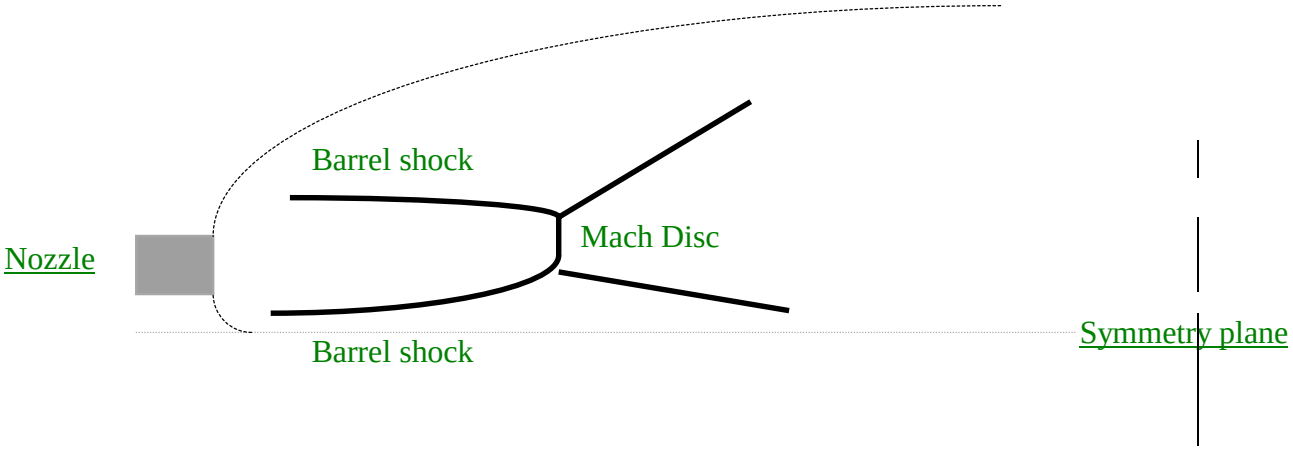

Figure 2.2a – Flow Structure of a Twin Supersonic Plume: Top View

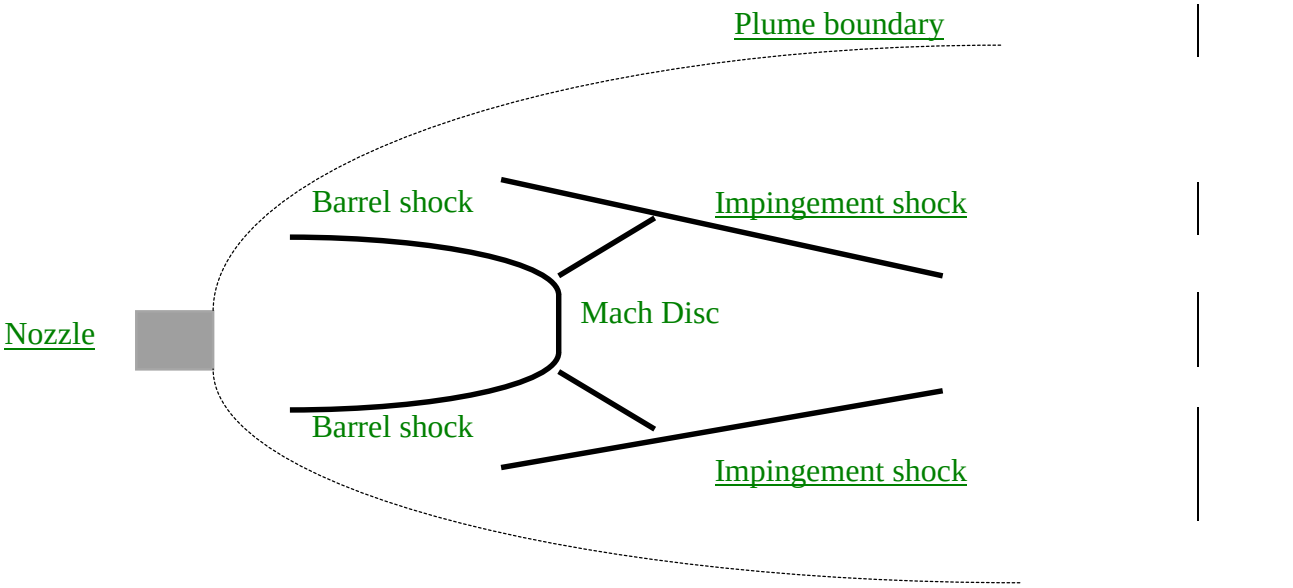

Figure 2.2b – Flow Structure of a Twin Supersonic Plume: Side View

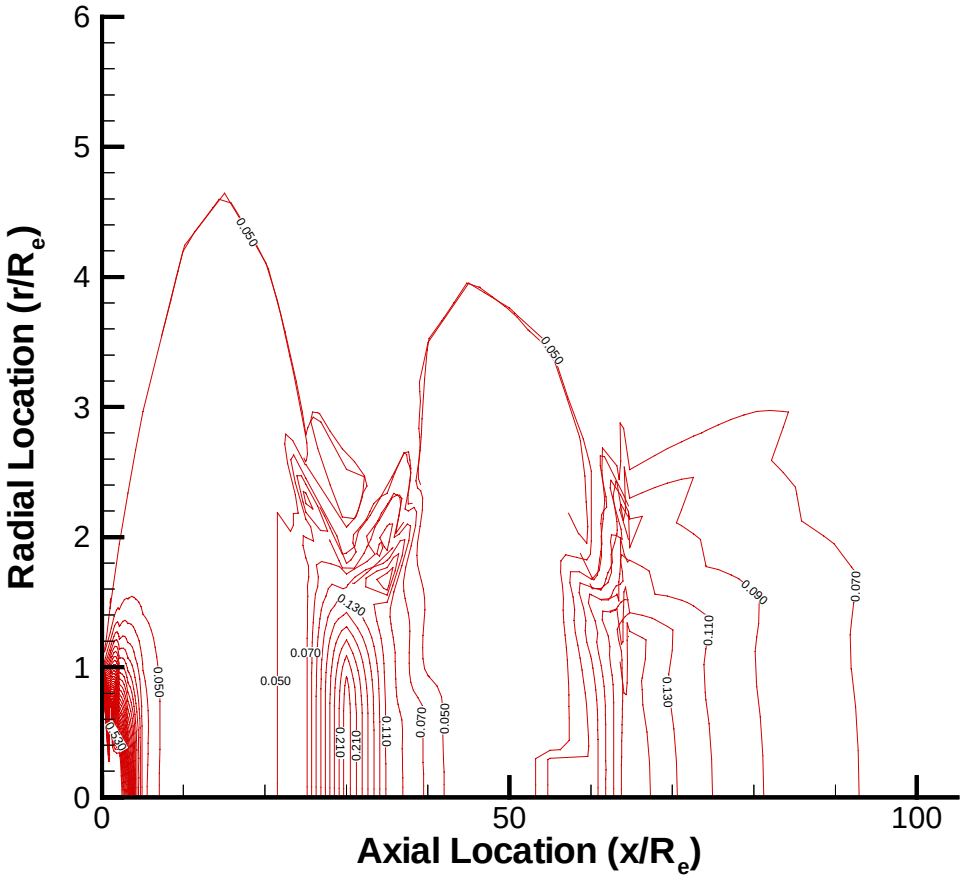

Figure 2.3 - Pressure Profile (Atm) for Titan IIIC Exhaust in Nearfield

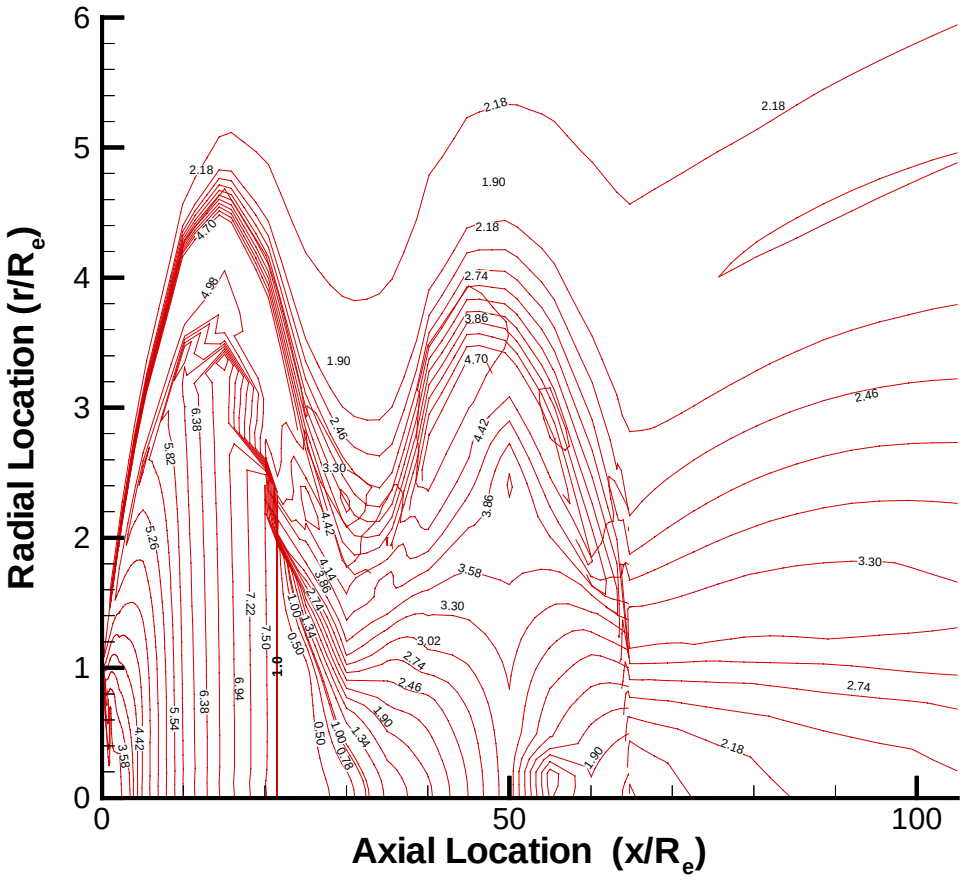

Figure 2.4 - Mach Number Profile for Titan IIIC Exhaust in Nearfield

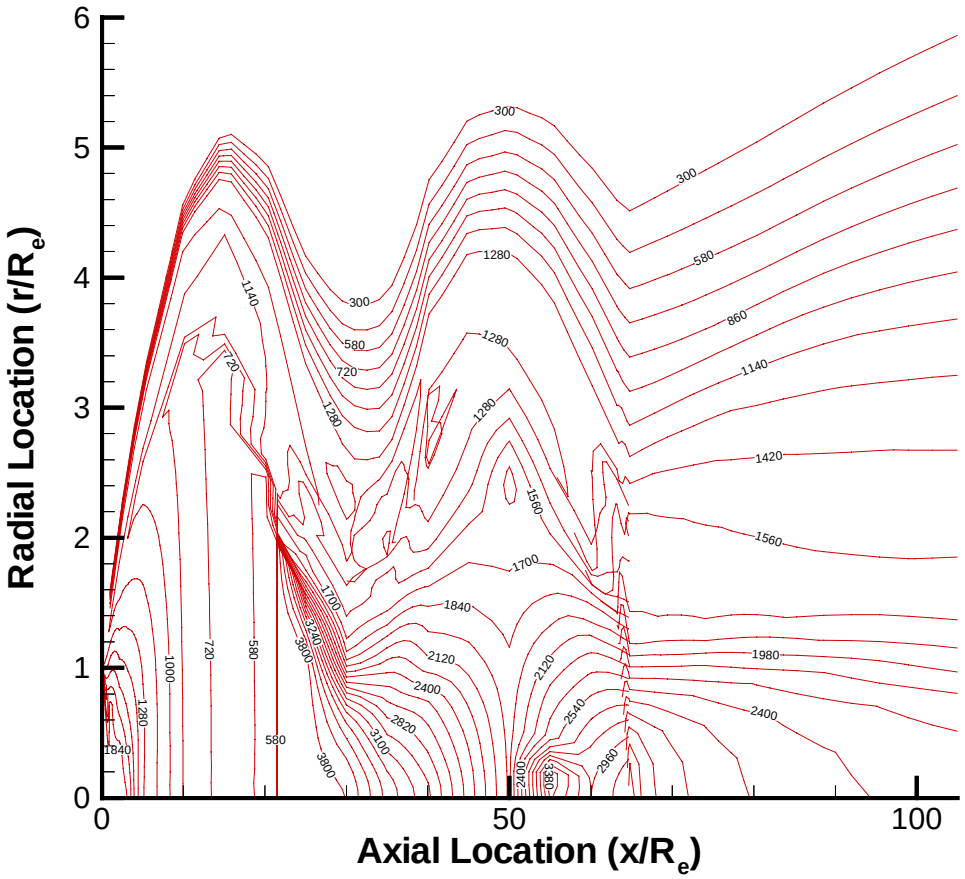

Figure 2.5 - Temperature (K) Profile for Titan IIIC Exhaust in Nearfield

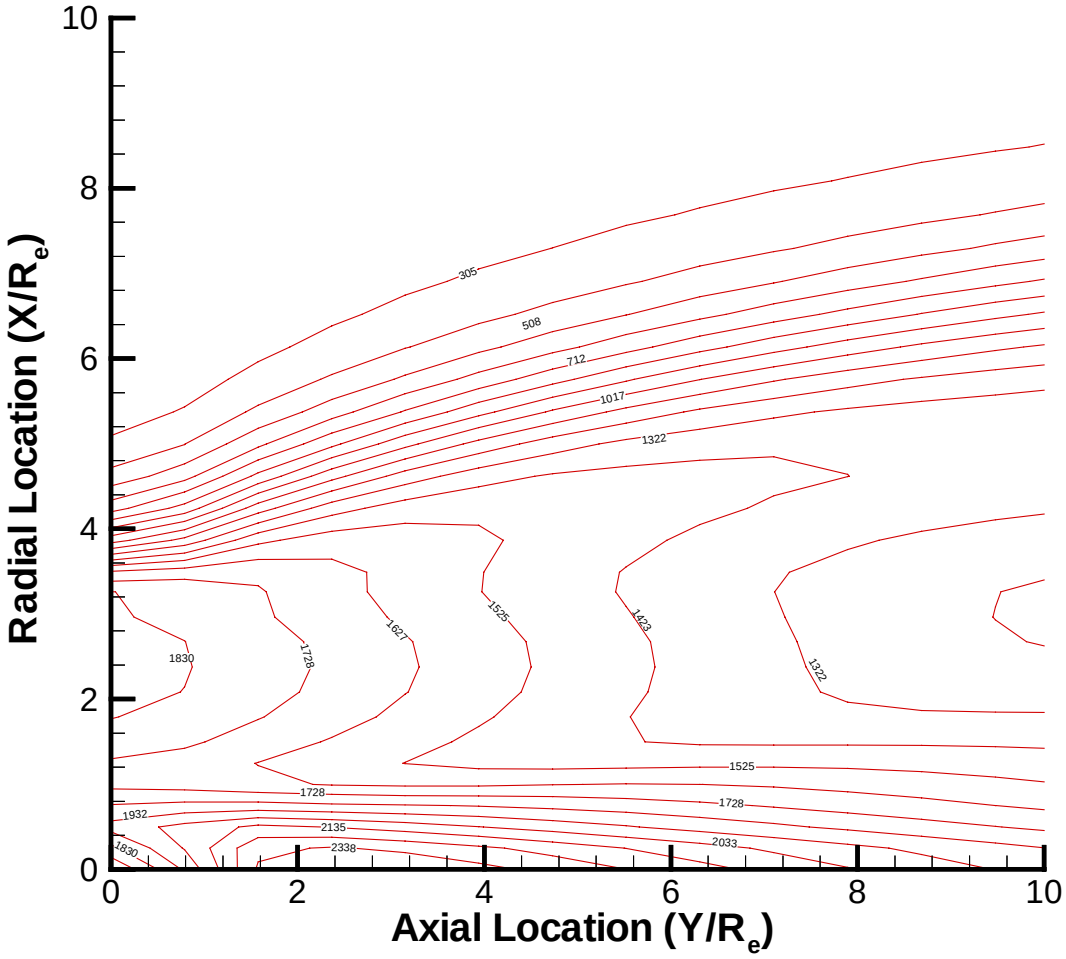

Figure 2.6 - Temperature (K) Profile for Titan IIIC Exhaust in Plume-intersecting Region

3. Stratospheric Ozone Depletion Caused by an SRM Launch

Ozone loss caused by an SRM passing through the stratosphere was evaluated by calculation at altitudes of 15, 20, 25, 30, 35, and 40 kilometers. The launch trajectory (for 2.4 Mlbf thrust level) was verified by comparison with several sources and is described in Reference 1.3. The state variables (velocity, altitude) are used to drive a SPF (Standard Plume Flowfield computer model) plume flowfield calculation. SPF is used to calculate the exhaust plume ("hot plume") from the nozzle exit plane to the location where the plume (by mixing with the ambient atmosphere) reaches dynamic and thermal equilibrium with the atmosphere. Inputs to the SPF "hot plume" calculation are vehicle altitude and nozzle exit plane conditions (species concentrations, velocity, temperature, pressure and relative speed between the ambient atmosphere and the exhaust plume velocity). The relative speed drives mixing in the shear layer (the mixing layer between the atmospheric gas and the exhaust plume). Mixing with the atmosphere spreads the plume and brings it to rest and results in a "cold wake" that is in thermal and dynamic equilibrium with the ambient gases. Mixing of the burnable plume species with ambient oxygen (afterburning) produces thermal decomposition of HCl into chlorine. The chlorine mechanism is the main cause of ozone destruction by SRM exhaust. The production of chlorine by afterburning is thus a key step towards ozone destruction and requires careful evaluation of the "hot plume" dynamics and chemistry (References 1.3 & 1.4 discuss the afterburning mechanism).

Additional Considerations

Two additional effects are included, the first being the increase in HCl decomposition caused by shock formation in the near-field including multiple engine plume interactions (as discussed in Section 2), and the second being the effects of cross wind.

Cross wind effects are examined by computational fluid dynamics analysis of flow of N_2 over a column of quiescent oxygen (a 200m square column). The full Navier-Stokes FLUENT computer code was used to examine the effects of cross-flow shear on the topography of the shape or aspect ratio of the exhaust plume cross section. The effect of the interaction of the flowing nitrogen on the oxygen is shown at two times (529s and 1357s) in Figures 3.1 and 3.2. Both the 529 second and 1357 second result show an elongation of the oxygen column. The elongation is caused by a combination of convection, shear, and forces and velocities driven by the aerodynamic like interaction (initially, the N_2 flow is like that around an obstacle) of the flowing nitrogen with the initially quiescent oxygen. (Laminar mixing was used for this particular calculation—turbulent mixing would further diffuse the O_2 column but the elongation will be similar to that calculated here.) The most important result of the cross flow interaction is to reduce the characteristic mixing length of the plume by elongation—the characteristic mixing length is the minor axis of the stretched column. As outlined in References 1.3 and 1.4, the effect of reduced characteristic length is to cause slower diffusion: the apparent eddy diffusion coefficient is proportional to the plume size ($K = br$, where K is the apparent eddy diffusion

coefficient, r is plume radius and b is an empirically-derived coefficient between 0.6 and 1.3). The present analysis does not determine the value b but leads to the selection of the lesser value of 0.6 (which results in the slowest diffusion within the empirically determined range discussed in Reference 1.4) to approximately account for the effects of cross wind on the diffusing cold wake. The significance of this result is to allow extension of the analysis discussed in References 1.3 and 1.4 where the results were limited to the few minutes after launch and before cross winds start to distort the cold wake from a circular cross section. The inclusion of the effects of cross winds (albeit in an approximate way) allows extension of the present results to times on the order of one to two hours.

Results of Analysis of Local Ozone Depletion (Cold Wake)

Results of the cold wake calculation are shown in Figures 3.3 through 3.14. The calculations are for altitudes from 15 to 40 km and show the concentrations of several species along the plume centerline as a function of time as well as the radial profile of species as for selected times. The present calculations are driven by analysis of the hot plume with afterburning taken into account as described in Reference 1.3 and accounting for near field and multiple engine effects discussed in Section 2. The analysis proceeds as follows:

1) The SPF model is used to calculate the hot plume with high temperatures caused by afterburning.

2) Conversion of HCl to Cl takes place in the high temperature afterburning region. Additional conversion of HCl to Cl caused by near field shock effects and multiple engine interaction shocks are included (about a 6% effect).

3) We use a conservative value for NO_x levels by assuming that all NO_x in the high temperature combustor flows into the plume. A more precise approach would account for depletion of NO_x in the thruster nozzle (as a result of decrease of temperature in the subsonic-supersonic flow) and we would evaluate the subsequent reformation of NO_x in the hot plume. The only plume contributor to NO_x reformation is the Mach disk (both afterburning and oblique barrel and multiple plume interaction shocks drive temperatures less than 2000K and the Zeldovich mechanism will not produce NO_x). Only a small fraction of the plume exhaust passes through the Mach disk. Thus the present approach is conservative as determined by the analysis of Section 2: we overstate the cold wake NO_x levels.

The wind shear-driven revision to the apparent eddy diffusion model is included in these calculations. The main interest of the present calculation is in the “early to medium time” diffusion-driven behavior which occurs within an two hours after launch (and before ambient ozone diffuses back into the wake). As the ozone hole increases in size ozone back-fills (as caused by diffusion processes) into the hole as time passes and the ozone concentration at the axis eventually recovers the ambient value. The process is controlled by the rate at which plume species diffuse into the ambient atmosphere. The process of ozone loss is controlled by the

reaction of ozone with chlorine (with ClO as a product) and the subsequent re-production of chlorine by photo reactions and reactions associated with ClO. It is this cyclic regeneration of Cl that causes the generation of an ozone hole (for the present SRM chlorine has a far greater effect on local ozone depletion than NO & NO_2 or aluminum oxide particles). In an average sense, on the order of ten ozone molecules are consumed by each original plume chlorine atom during this early time before diffusion fills up the hole. The total loss of ozone is somewhat greater than the size of the hole indicates since the hole begins to fill when the radially-inward diffusion of ozone exceeds the ozone loss.

Results for ozone loss calculations are shown in Figures 3.3 to 3.14. The centerline values of several species are shown. The time to "fill the axis" with ambient ozone is seen to take between 3000 seconds at 15-20 km to about 6000 seconds at 40 km.

The detailed behavior of the diffusing, reacting plume is complex as can be seen from examination of Figures 3.3-3.14. The process is controlled by the rate at which plume species diffuse into the ambient atmosphere (a process that is slowed by the stretching caused by cross winds and modeled as a reduction in apparent turbulent eddy diffusivity). The initial cold wake size (radius) varies from 150 m at 15 km to 650m at 40 km. The combination of size differences and ambient atmosphere pressure lead to a larger local ozone hole that lasts longer at higher altitude. Examination of the figures show the loss of ozone at the "diffusion interface" where the process of ozone loss is controlled by the reaction of ozone with Cl (with production of ClO and Cl_2O_2), and the subsequent reproduction of chlorine atoms by photo reactions and reactions associated with ClO and Cl_2O_2 (both found in high concentration in the ozone hole region). Comments regarding selected figures are helpful in understanding the ozone hole behavior.

1) Figure 3.4: The radial species distribution is given at 2466 s which is near the end of the lifetime of the ozone hole. The hole is nearly filled up and the radius is approximately 3500 m.

2) Figure 3.5: The local ozone hole is seen to last about 2500 seconds at 20km.

3) Figure 3.9: The 30 km ozone hole has a lifetime of 4500 s. Examination of Figure 3.10 shows the ozone hole approaching its maximum size of radius 6000m.

4) Figures 13 & 14: The local ozone hole (the initial cold wake has a radius of 650 km) approaches a size of 20 km with a lifetime of 5000 s.

A measure of the ozone hole size (and age) is made by taking the time at which the centerline value is about 25% of the ambient value and the location where the ozone concentration is approximately 90% of the ambient value. These values are shown in the following table:

Table 3-1. Ozone hole size (radius) and lifetime in the stratosphere.

Altitude, km	Ozone Hole Lifetime, s	Ozone Hole Size , m
15	2500	3500
20	2500	3000
25	2500	3000
30	4500	6000
35	5000	7000
40	5000	20000

The present local ozone calculations are in excellent agreement with the fly-through measurements of the local depletion for a Titan IV as reported in Reference 3.1 and discussed further in Reference 3.2. The measurements were made at the 17.4 km and determined the following ozone hole characteristics:

- ozone hole diameter 6 km
- duration or life of hole is 3000 seconds.

The present analysis projects an ozone hole diameter of 2 x 3250 = 6500 meters with an ozone hole lifetime of 2500 seconds.

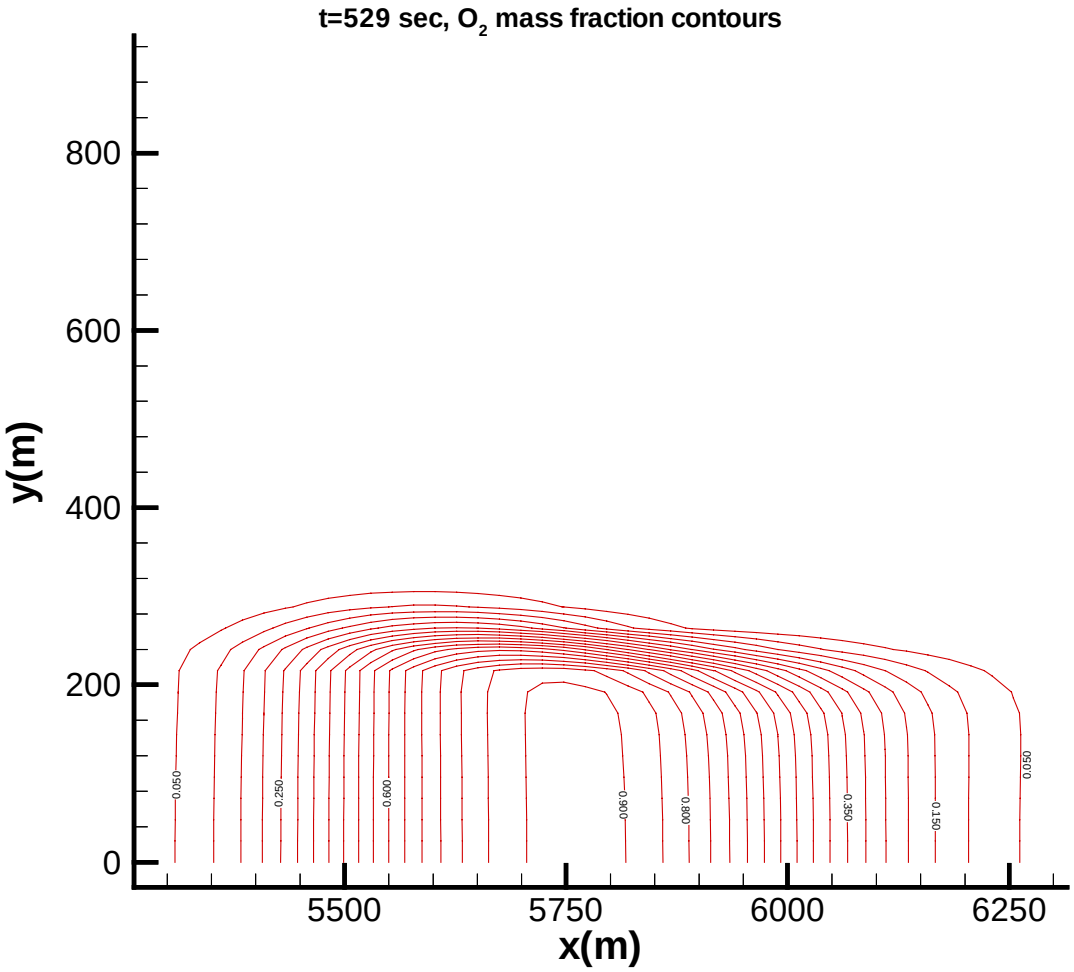

3.1 - Figure Plume mass contours at 529 seconds: 1.5 m/s wind.

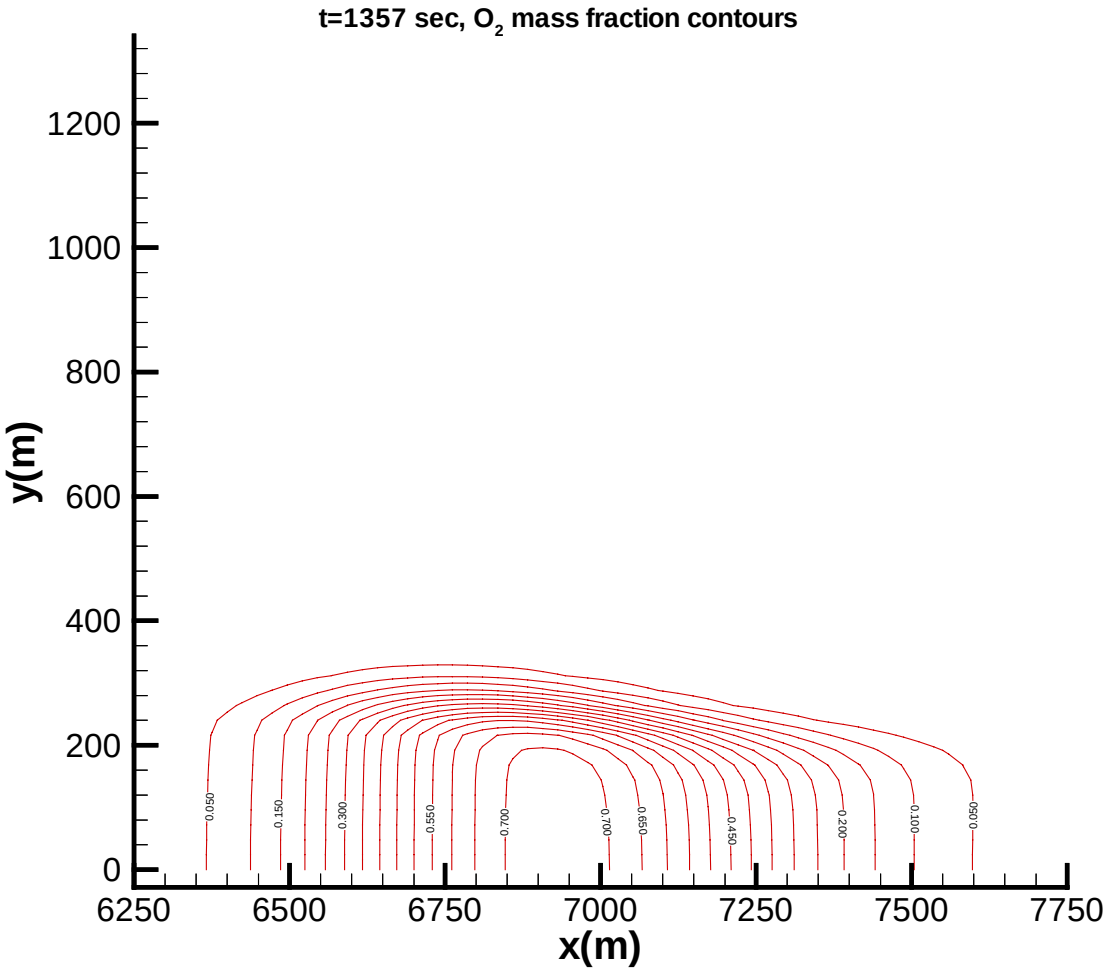

Figure 3.2 - Plume mass contours at 1357 seconds: 1.5 m/s wind.

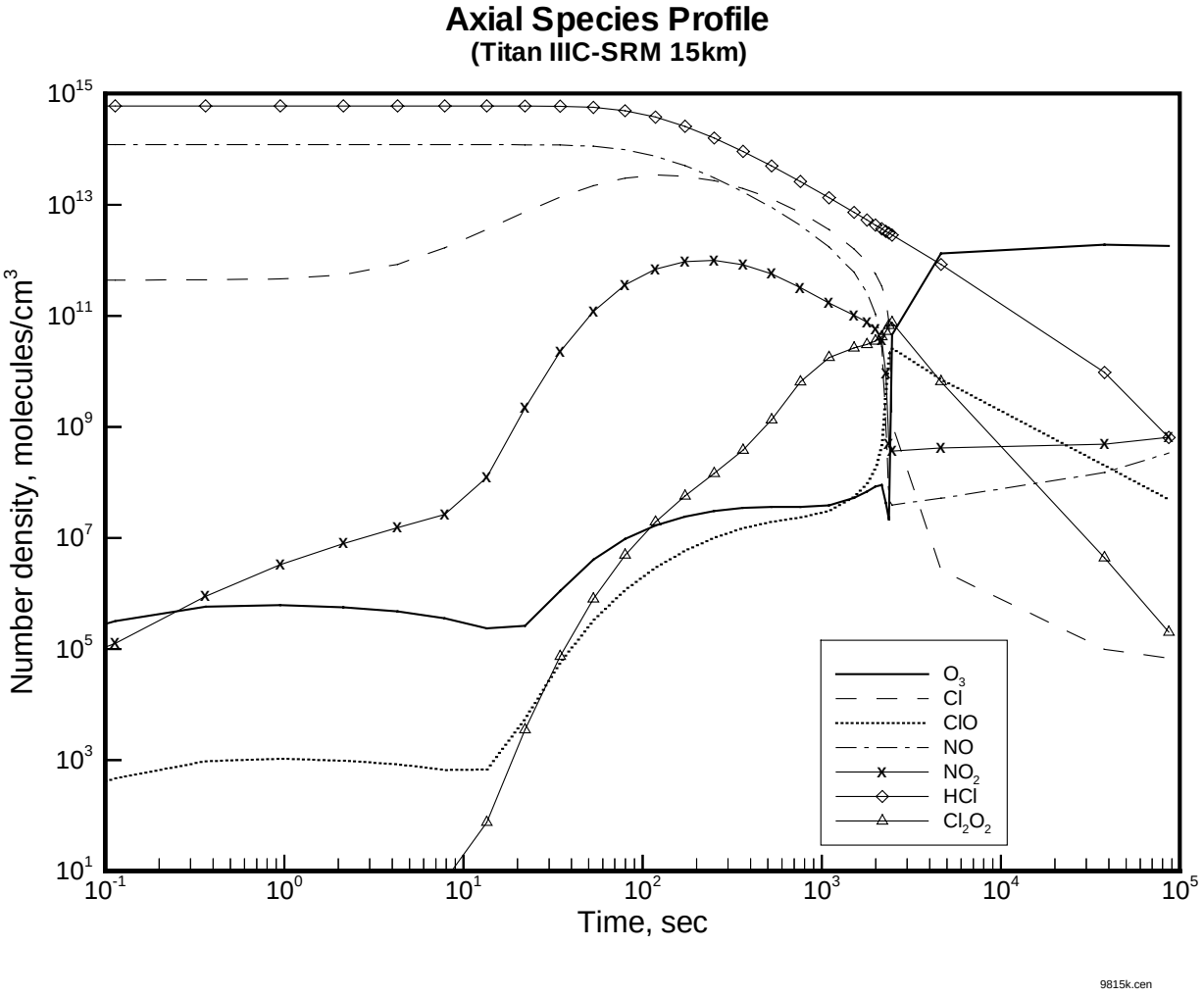

Figure 3.3 - Centerline Concentrations: 15 km.

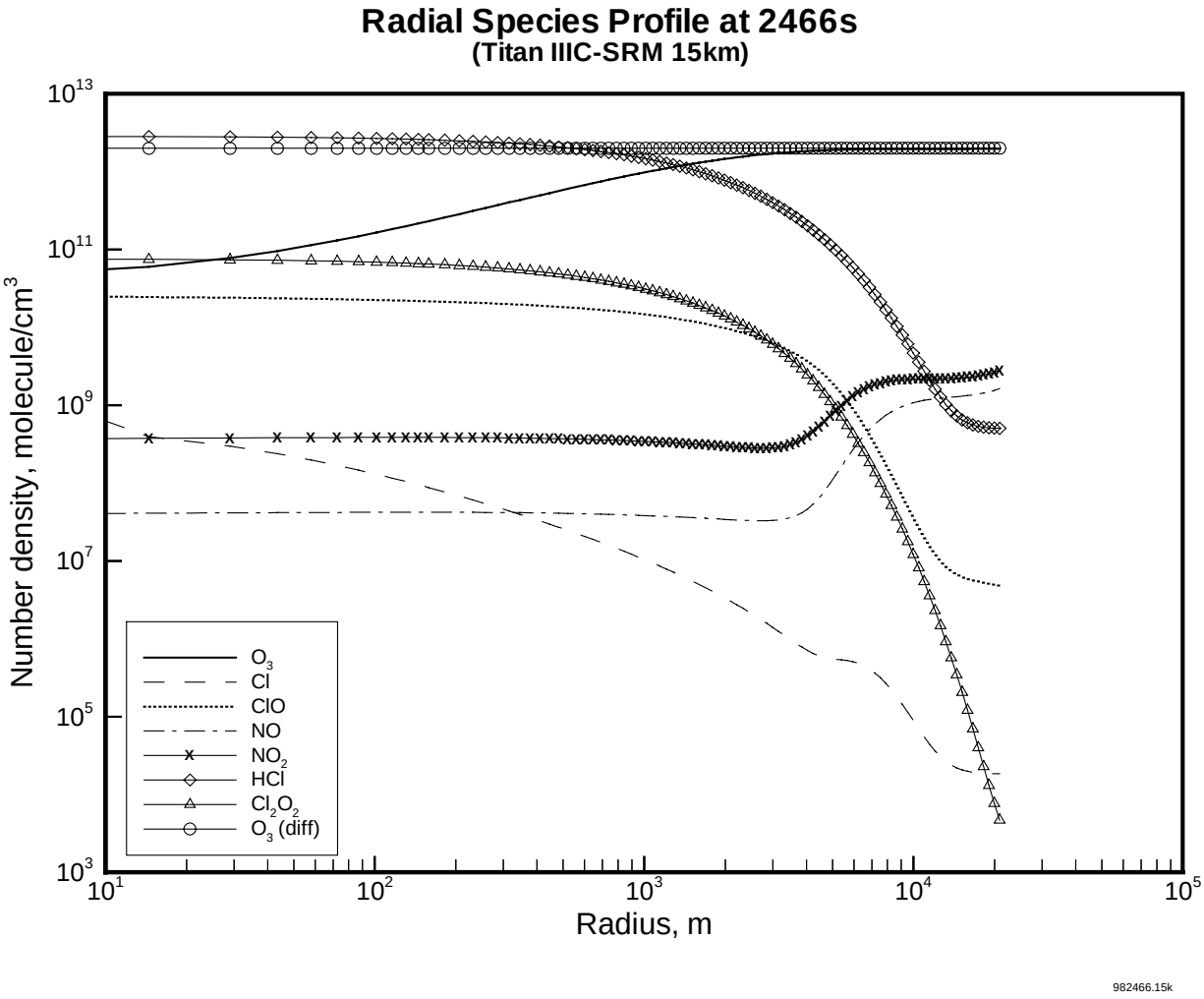

Figure 3.4 - Radial Concentration Profiles: 15 km, 2466s.

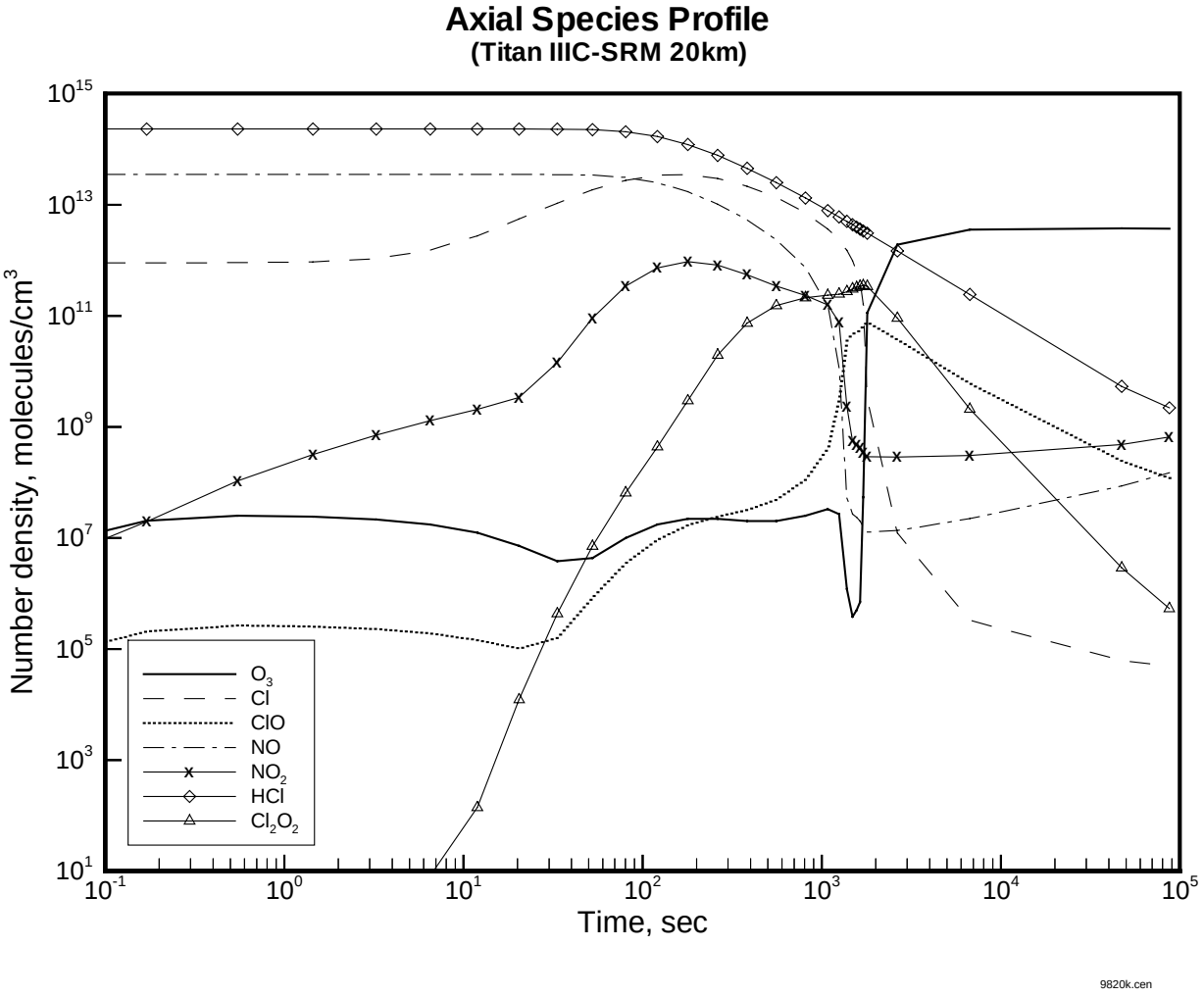

Figure 3.5 - Centerline Concentrations, 20 km.

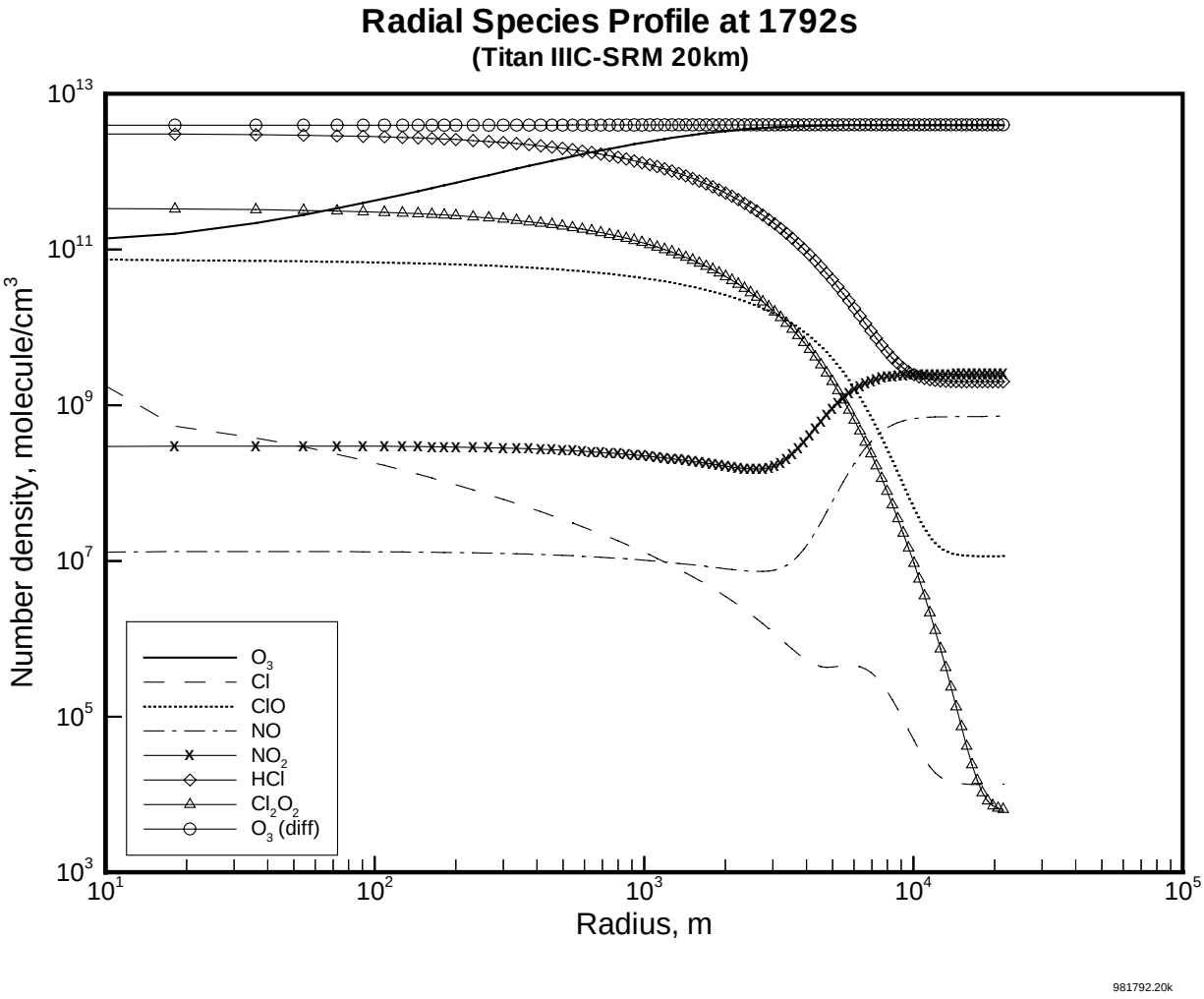

Figure 3.6 - Radial Concentration Profiles, 20 km, 1792s.

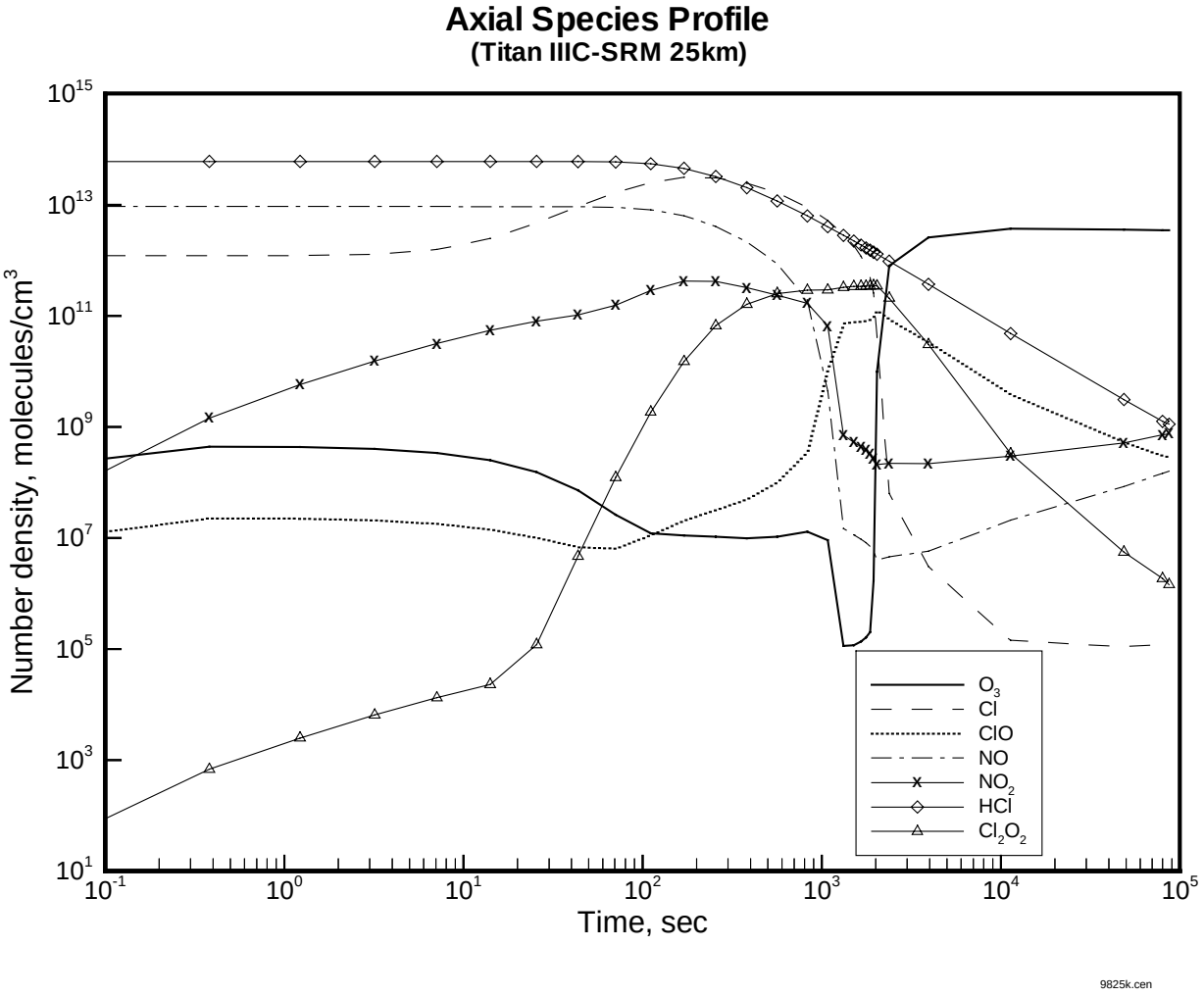

Figure 3.7 - Centerline Concentrations: 25 km.

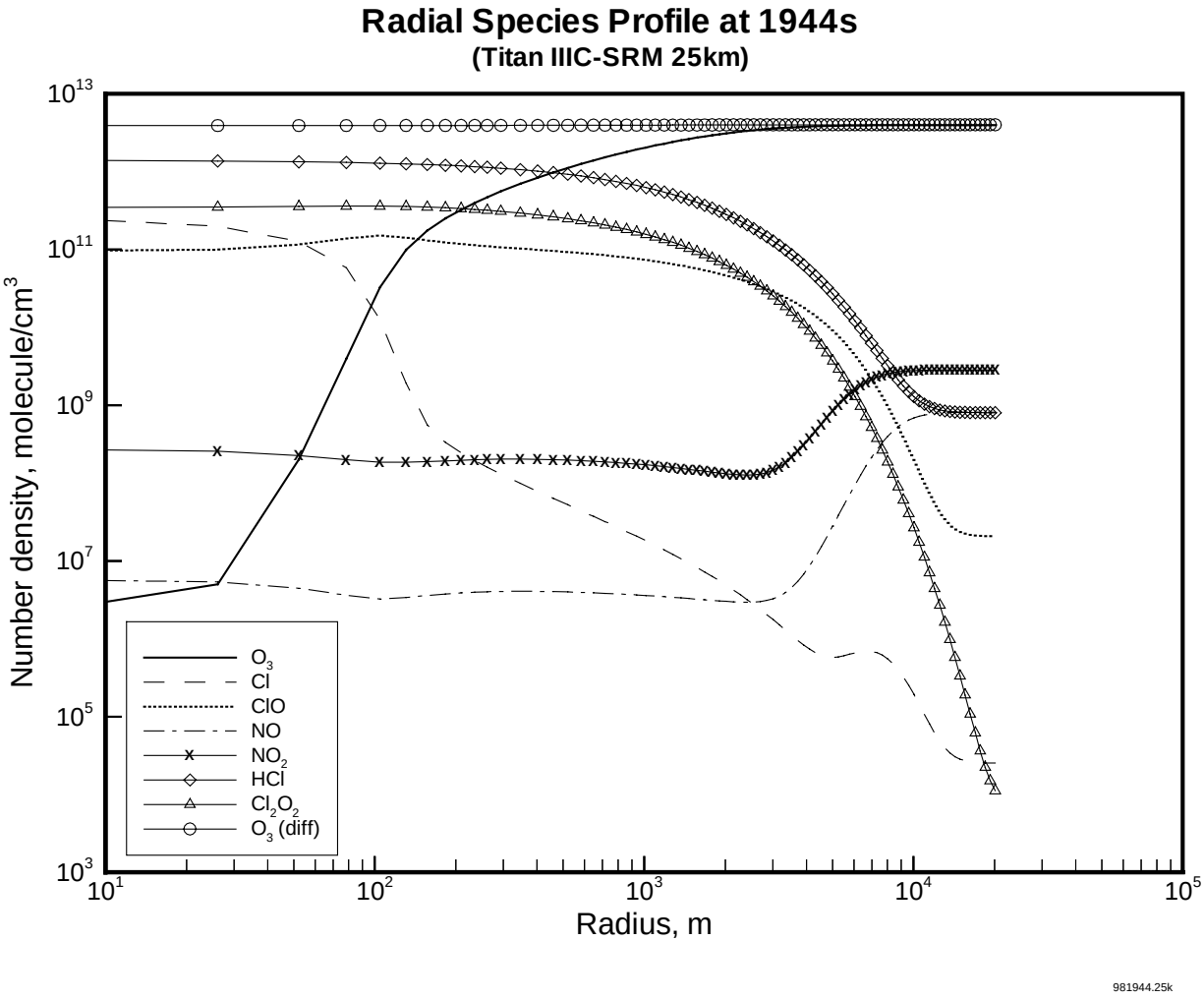

Figure 3.8 - Radial Concentration Profiles: 25 km, 1944s.

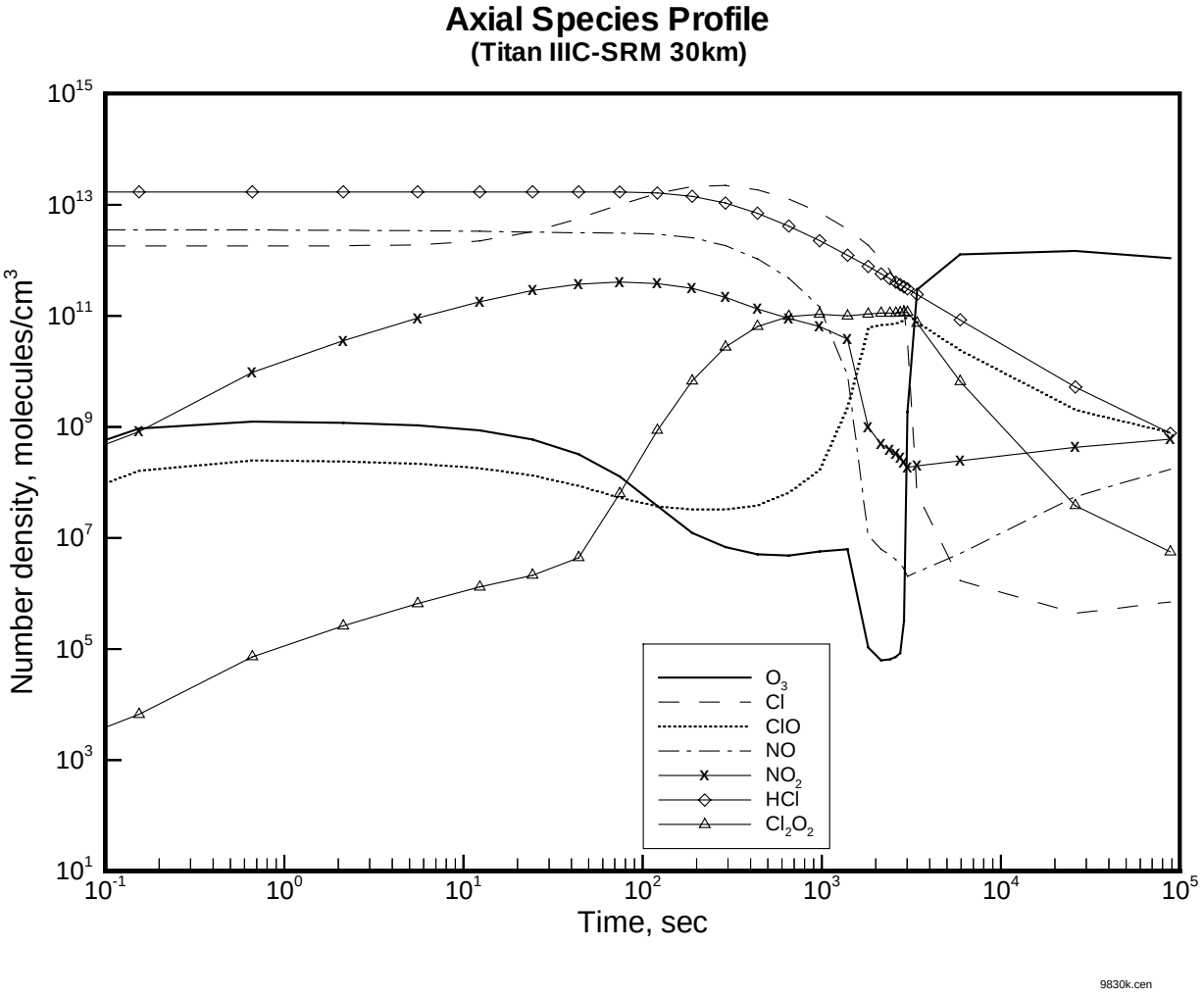

Figure 3.9 - Centerline Concentrations: 30 km.

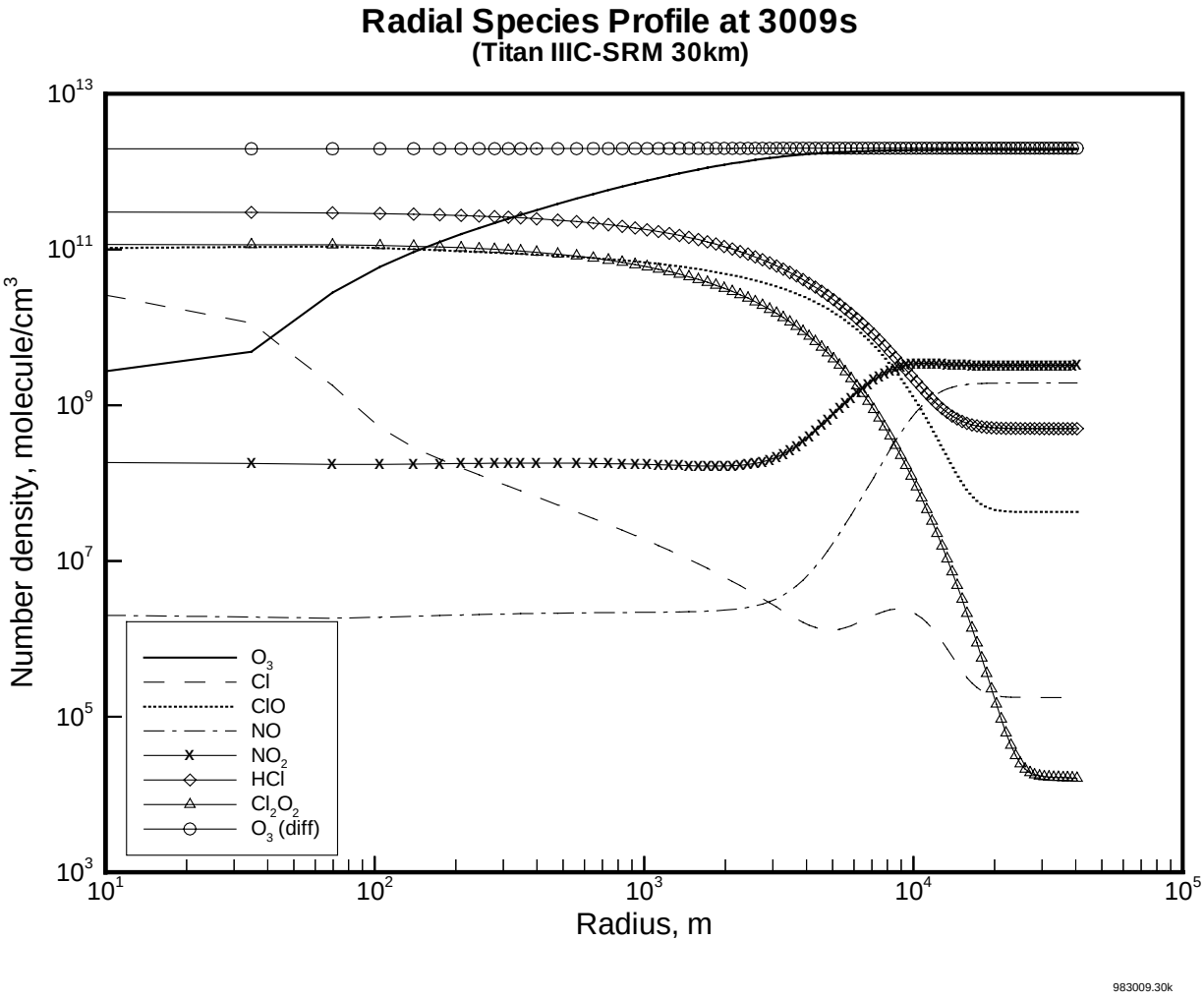

Figure 3.10 - Radial Concentration Profiles: 30 km, 3009s.

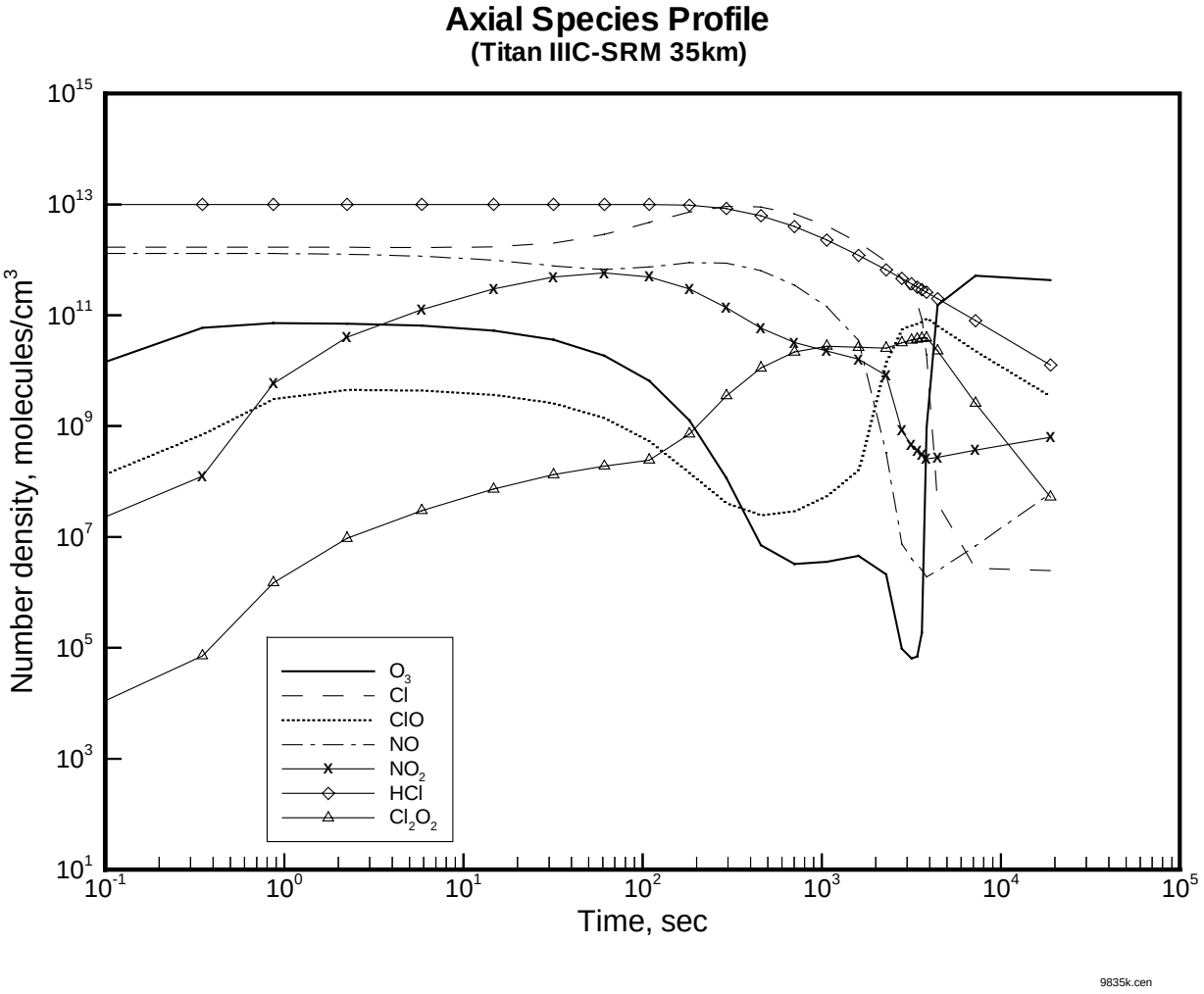

Figure 3.11 - Centerline Concentrations: 35 km.

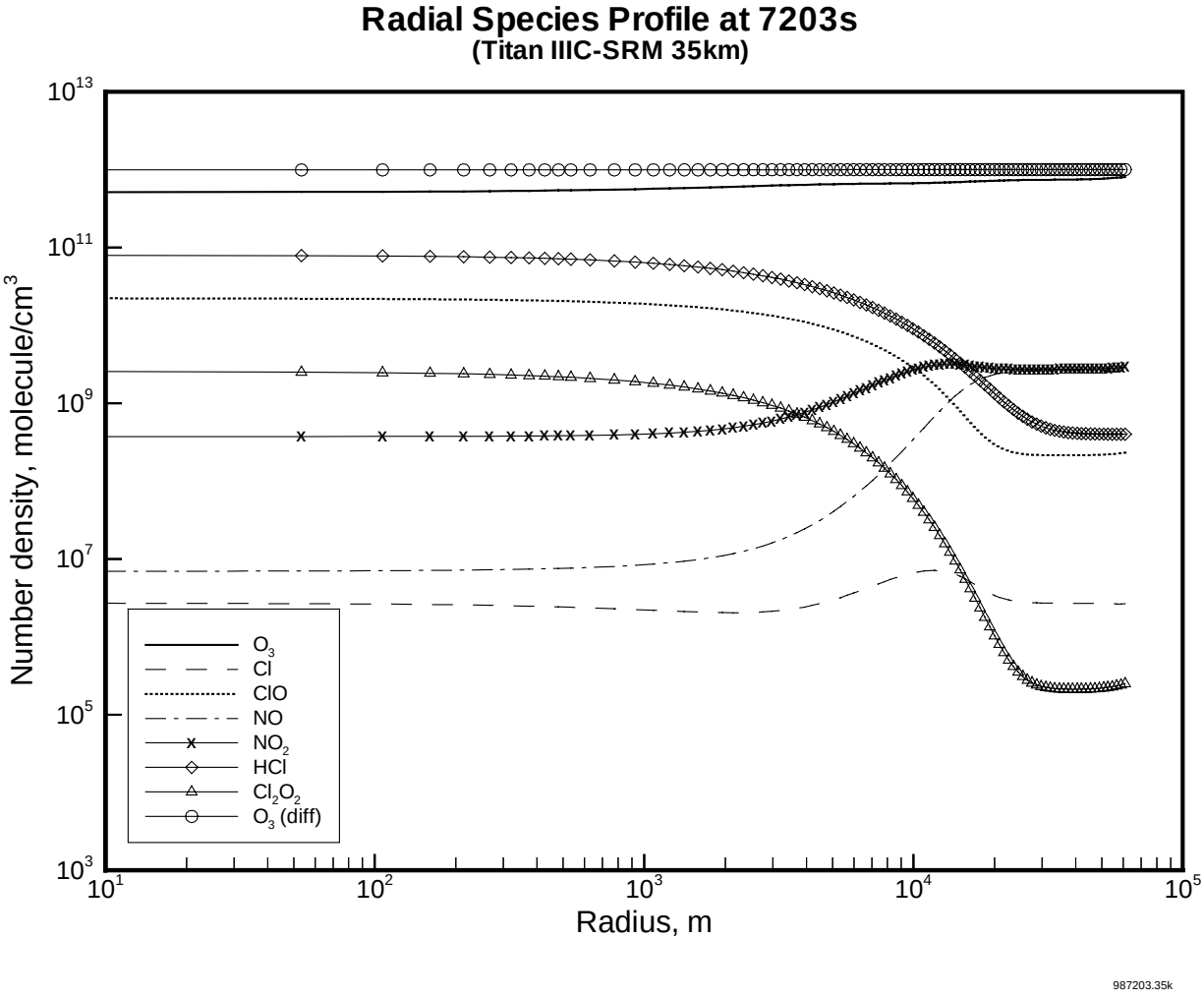

Figure 3.12 - Radial Concentration Profiles: 35 km, 7203 s.

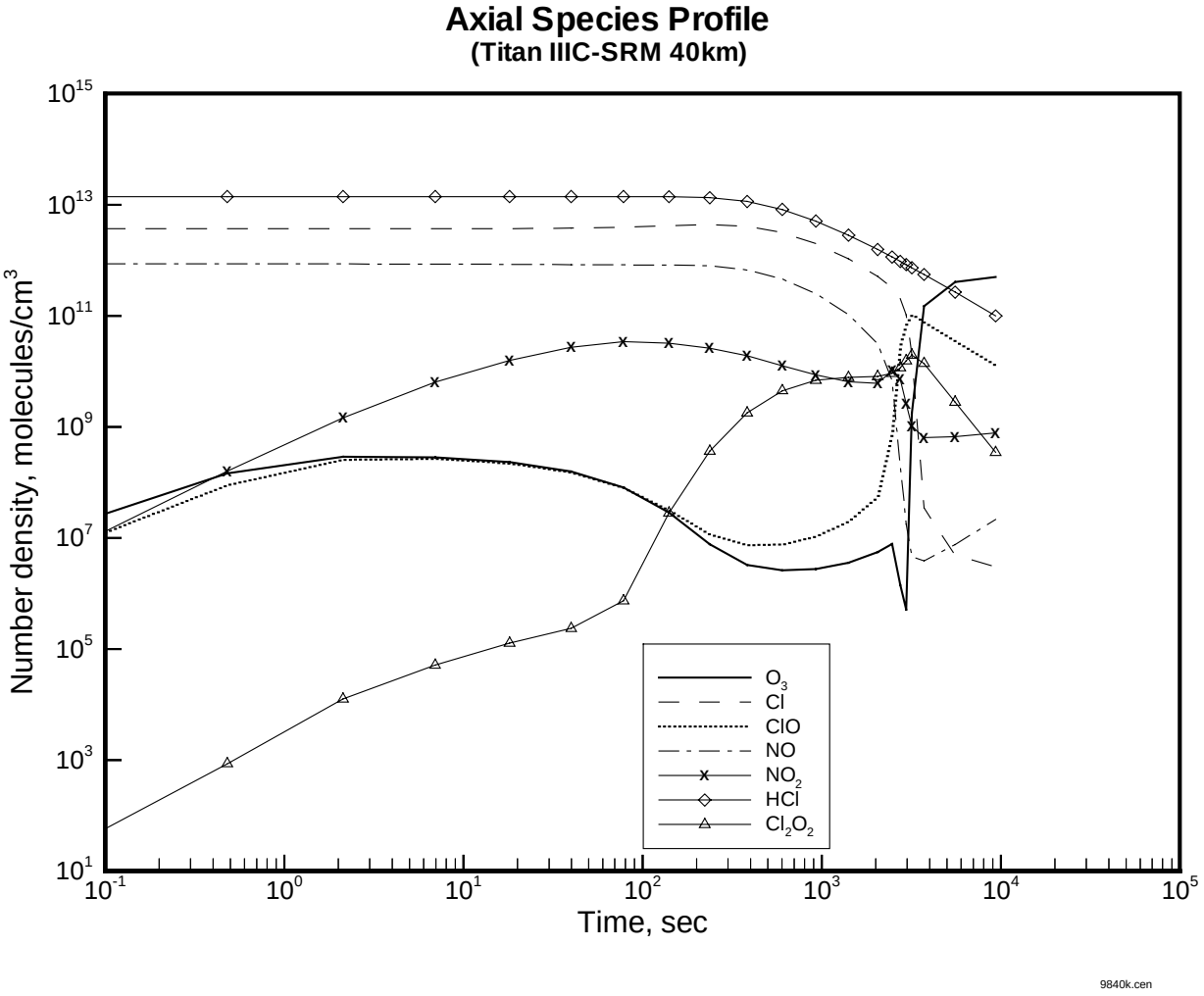

Figure 3.13 - Centerline Concentrations: 40 km.

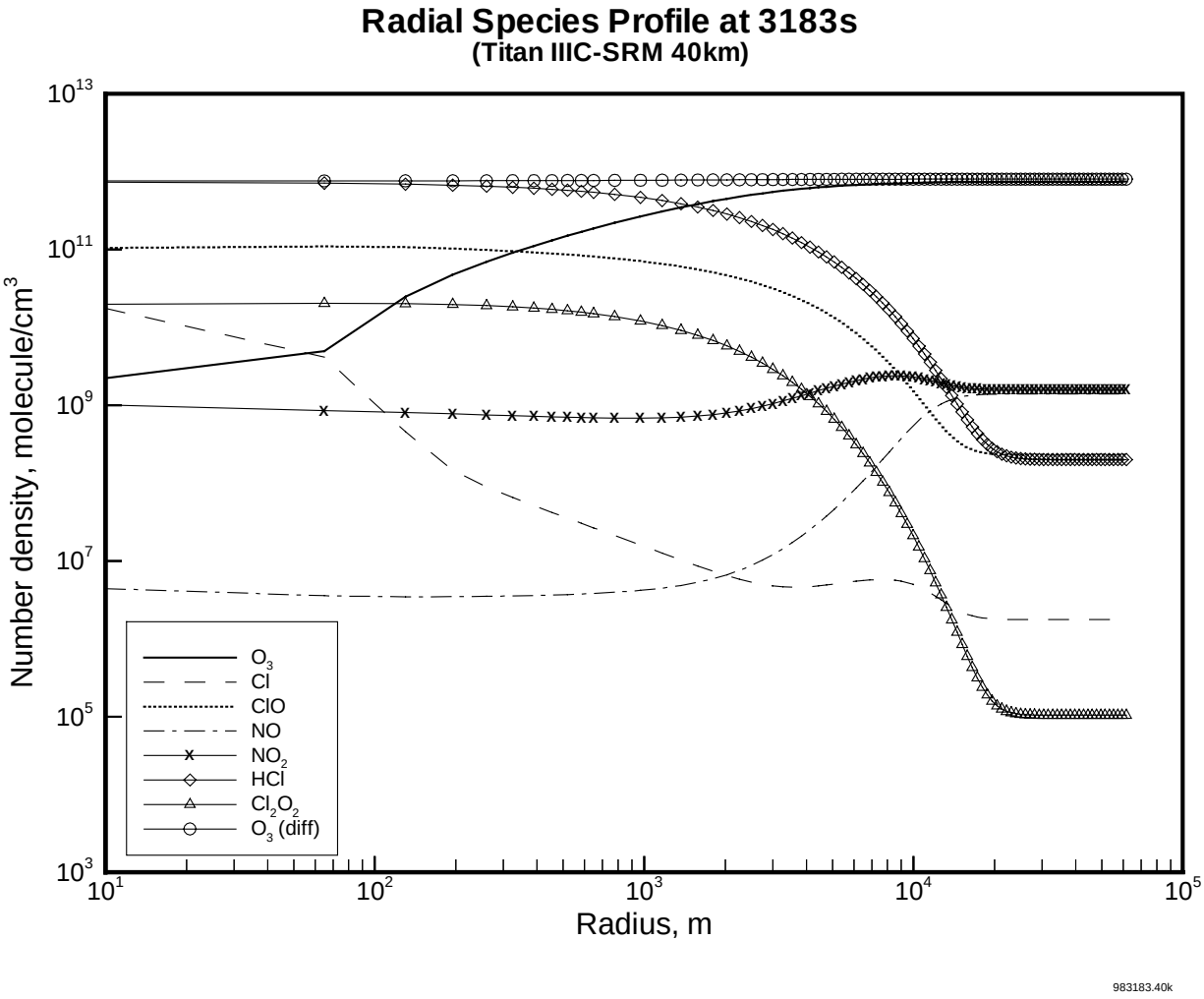

Figure 3.14 - Radial Concentration Profiles: 40 km, 3183s.

4. Summary and Discussion

Methodology for calculation of ozone depletion caused by rocket launches has been upgraded and applied to a solid rocket launch of a (two motor) Titan IV. Near-field plume shocks and multiple engine effects were accounted for as were the effects of cross winds on the diffusion rate. The selection of the apparent eddy diffusion coefficient was chosen at the lower end of the experimentally determined range (Reference 1.4) in order to account for cross wind effects. Attention was restricted to the local ozone depletion within an hour or two after launch. (Estimates of global impact are unchanged from those reported in Reference 1.3.)

The upgraded methodology was applied to several altitudes in the stratosphere and for a launch with a 2.4 Mlb SRM thruster (two 1.2 Mlb SRM's). Estimates were made on both the local ozone hole for times in excess of one hour. The present results are in agreement (see Table 4-1) with the recently measured local ozone depletion caused by Titan IV launches (Reference 3.1):

Table 4-1. Comparison of of *In-Situ* Versus Current Model Ozone Depletion

Altitude (17.4 km)	*In-situ* measurement	Present model
Ozone Hole Size	6 km	6.5 km
Ozone Hole Lifetime	3000 s	2500 s

The present selection of the apparent eddy diffusion coefficient was driven by cross wind considerations. The effect of cross wind will be more pronounced if the cross-wind has a vertical velocity variation. Differential "stretching' and convection along the cold wake vertical column will result in the "pinching off" of the column into discrete cylinders of length inversely proportional to the velocity gradient along the column and directly proportional to the column velocity. The remnant exhaust volumes will diffuse and convect forming local pockets of depleted ozone. The size and life of the pockets will vary with their initial size. Their formation and location depends on the local wind profile that fluctuates greatly with time. However, the ozone column effect from the individual volumes is expected to be relatively small and the overall effect is not be expected to be additive over any significant number of volumes: hence the column effect from a uniform cross wind with no gradient, which tends to not break up the plume column, will project the largest local decrease in ozone column. The present analysis considers uniform cross wind and hence is conservative.

5. Recommendations

During the last decade the space community has witnessed an explosion of space activities in the military as well as the commercial arena. Particularly in the telecommunication area the demand for new space vehicles has increased by several hundred percent. Equipped with the knowledge of the various ozone depletion mechanisms we propose the following tasks in order to assess the impact on stratospheric ozone as a result of sky-rocketing space activities:

(1) Assessment of the effect on stratospheric ozone resulting from planned or unplanned destruction of SRM as well as liquid launch vehicles. The impact on ozone caused by combustion/explosion of solid propellant can be similarly characterized as in our previous works, i.e. assessment of HCl production and its subsequent fate in terms of dissociation into chlorine. The impact from the liquid engine explosion/combustion however depends on the production of H_2O, H, HO and HO_2, etc. It is well known that ozone can be consumed through the HO_X mechanism:

$$HO + O_3 \rightarrow HO_2 + O_2 \qquad (5\text{-}1)$$

$$HO_2 + O_3 = HO + 2\,O_2 \qquad (5\text{-}2)$$

(2) Assessment of the transport of exhaust gases produced by spacecraft functions such as fuel dumps, station keeping, pointing, and drag makeup. As a result of increased space activities large amount of effluents released in high altitude will diffuse and potentially be transported downward through the thermosphere and mesosphere into the stratosphere. These effluents upon arriving in the upper stratosphere may undergo catalytic cycles e.g. the NO_X and HO_X cycles, to deplete ozone.

(3) A statistical evaluation of the cross wind gradient effect on both local ozone depletion and global ozone depletion. The task would use computational fluid dynamics to quantify the column dynamics and "pinching" effects under a set of typical stratospheric wind profiles. The, anchored, cold wake model would be used to calculate column and "pinched off" volume ozone depletion and the outputs of the local depletion analysis would be used to upgrade global impact estimates.

(4) A compilation of the impact of all launch vehicles on stratospheric ozone. This task will employ the methods described in this report with the enhancement from the #3 proposed task. Both solid and liquid boosters will be included. Local and global impact will be assessed.

References

1.1 "The impact of Deorbiting Space Debris on Stratospheric Ozone", P. D. Lohn, E. Y. Wong, M. J. Molina, M. R. Denison, J. J. Lamb, Prepared by TRW for Space and Missile Systems Center, May 31, 1994.

1.2 "Utilization of Alternate Propellants to Reduce Stratospheric Ozone Depletion," Prepared by TRW for Space Defense and Missile Systems Center, May 31, 1994.

1.3 "The Effects of Rocket Exhaust on Stratospheric Ozone: Chemistry and Diffusion", P. D. Lohn & E. Y. Wong, Prepared for USAF Space and Missile Systems Center, August 1996.

1.4 Solid Rocket Exhaust in the Stratosphere: Plume Diffusion and Chemical Reactions", M. R. .Denison, J. L. Lamb, W. D. Bjorndahl, E. Y. Wong, P. D. Lohn; Journal of Spacecraft & Rockets, **v**31,**n**3, pages 435-442,May-June 1994.

2.1 "Computer Model Prediction of the Local Effects of Large, Solid-Fuel Rocket Motors on Stratospheric Ozone", P. F. Zittel, Aerospace Corporation Technical Report No. TR-94(4231)-9, 1994.

2.2 "Laboratory Generation of Free Chlorine from HCl under Stratospheric Afterburning Conditions", M.L. Burke & P.F. Zittel, Combustion and Flame, **v112**, 1998], p. 210.

2.3 "The Production of Nitric Oxide in the Troposphere as a Result of Solid-Rocket-Motor Afterburning," R. B. Stewart & R. I. Gomberg, NASA TN D-8137, 1976.

3.1 "In-situ Dual Beam UV Absorption Measurement of Ozone in SRM Plumes", J.R. Benbrook and W.R. Sheldon, AIAA-97-0528, Reno, January 1997.

3.2 "Observation of Stratospheric Ozone depletion in Rocket Exhaust Plumes", M.N. Ross, J.R. Benbrook, W.R. Sheldon, P.F. Zittel, and D.L. McKenzie, Nature, v390, November 6, 1997.